



# Lithospheric structure beneath the boundary region of North China Craton and Xing Meng Orogenic Belt from S-receiver function analysis

Fanchang Meng<sup>a,c</sup>, Yinshuang Ai<sup>a,c,d,\*</sup>, Tao Xu<sup>b,d</sup>, Ling Chen<sup>b,c,d</sup>, Xin Wang<sup>a,d</sup>, Long Li<sup>a,c</sup>

<sup>a</sup> Key Laboratory of Earth and Planetary Physics, Institute of Geology and Geophysics, Chinese Academy of Sciences, 100029 Beijing, China

<sup>b</sup> State Key Laboratory of Lithospheric Evolution, Institute of Geology and Geophysics, Chinese Academy of Sciences, 100029 Beijing, China

<sup>c</sup> College of Earth and Planetary Sciences, University of Chinese Academy of Sciences, 100049 Beijing, China

<sup>d</sup> Innovation Academy for Earth Science, Chinese Academy of Sciences, 100029 Beijing, China

## ARTICLE INFO

### Keywords:

North China Craton  
Xing-Meng Orogenic Belt  
Lithosphere–asthenosphere boundary  
Mid-lithosphere discontinuity  
S-receiver functions  
Pacific subduction

## ABSTRACT

The boundary region of the North China Craton (NCC) and Xing-Meng Orogenic Belt (XMOB), including the northern boundary of the NCC and the southern XMOB, is the ideal area to investigate the spatially uneven lithospheric deformation and associated tectonic evolution in the boundary region of the craton and orogen. The depths and structures of the lithosphere–asthenosphere boundary (LAB) and mid-lithosphere discontinuity (MLD) are the key information to describe the nature and deformation pattern of the lithosphere, and thus can provide basic constraints on the associated tectonic processes and mechanism of the lithospheric deformation. Based on waveform data collected from 226 broadband seismic stations, high resolution spatial variations in the LAB and MLD depths were obtained by using the wave equation migration method for the S-receiver functions. The migrated images show a lateral variation in the LAB depth from 100–120 km in the northern boundary of the NCC to 120–140 km in the southern XMOB. The imaged LAB within the NCC is much shallower than that revealed by mantle xenoliths enclosed in the nearby Early Paleozoic kimberlites (~180 km), suggesting that the cratonic lithosphere of the area may have undergone significant thinning during the Phanerozoic evolution. Furthermore, a coherent MLD is identified at depths of 70–90 km beneath the northeastern NCC, which corroborates the speculation that the MLD probably existed in the eastern NCC before lithospheric destruction in the Mesozoic. The spatial variations in the LAB and MLD depths probably reflect complex lithospheric deformation and thinning around the boundary region of NCC and XMOB. The properties, including the gradient thickness and S-wave velocity contrast, of the two discontinuities further indicate that lithospheric deformation and thinning might be related to partial melting induced by the Big Mantle Wedge associated with the subducting Paleo-Pacific plate and its stagnation during the Late Mesozoic.

## 1. Introduction

Determining the depth and physical properties of the lithosphere–asthenosphere boundary (LAB) is essential to our understanding of lithospheric deformation and plate tectonics. More specifically, the spatial variations in the depth of the LAB across and within different tectonic blocks, especially in the boundary regions of cratons and subduction zones, could provide insight into the heterogeneity of lithospheric deformation as well as the mechanism responsible for lithospheric modification and thinning. Additionally, understanding the seismic properties of the LAB, such as the velocity contrast and gradient, could reveal mechanical details of interaction between the lithosphere

and asthenosphere, including the temperature (Höink and Lenardic, 2010), changes in composition associated with metasomatism, and partial melting of the mantle. In addition to the LAB, the mid-lithosphere discontinuity (MLD), which is internal to the lithosphere, has been widely identified in stable continental and cratonic areas with a thick lithosphere (Abt et al., 2010; Chen et al., 2014; Ford et al., 2010; Foster et al., 2014). Although the nature and origin of the MLD are still uncertain, interpretations of the MLD generally consider the temperature, anisotropy (Karato et al., 2015; Selway et al., 2015), elastically accommodated grain boundary sliding (EAGBS) model related to the thermal induced transition, and changes of composition into account. The depth and properties of the MLD can reflect the structural history of

\* Corresponding author at: Key Laboratory of Earth and Planetary Physics, Institute of Geology and Geophysics, Chinese Academy of Sciences, 100029 Beijing, China.

E-mail address: [ysai@mail.iggcas.ac.cn](mailto:ysai@mail.iggcas.ac.cn) (Y. Ai).

<https://doi.org/10.1016/j.tecto.2021.229067>

Received 7 February 2021; Received in revised form 29 June 2021; Accepted 16 September 2021

Available online 22 September 2021

0040-1951/© 2021 Elsevier B.V. All rights reserved.

a continent, and its influence on the long-term evolutionary properties of continents. Collectively, the depth and physical properties of the LAB and MLD could thus reveal imprints on the lithospheric structure left by tectonic evolution in target regions.

The boundary region of the North China Craton (NCC) and Xing-Meng Orogenic Belt (XMOB), including the northern boundary of the NCC (which is composed of the Liaodong tectonic belt and Tanlu Fault Zone) and parts of the XMOB (which is composed of the southern Xing'an block and Songliao Basin), is located in the westward subduction zone of the Paleo-Pacific plate (Fig. 1). The special geographic location of the boundary region of NCC and XMOB makes the region an ideal place to investigate the spatial variations of lithospheric structure and their associated deformation and tectonic evolution in the boundary region of the NCC and the Paleo-Pacific plate subduction zone. The NCC shows features indicative of remaining thick lithospheric mantle roots and the MLD in its middle and western parts, while the NCC has been severely destroyed and reformed in its eastern part since the Phanerozoic (Zhao, 2005; Zheng et al., 2006; Xu, 2007). Deformation and destruction of the lithospheric structure in the NCC not only changed its inner structural patterns and deep structures but also inevitably left evolutionary imprints on its boundary zones and adjacent areas, such as the northern boundary of the NCC and adjacent regions. Furthermore, crustal compression, crustal extension and associated thinning (Wang et al., 2014; Tang et al., 2018), basin development, and wide distribution of volcanic rocks from the late Mesozoic to Cenozoic (Wang et al., 2006; Zhang et al., 2006, 2015) make the evolutionary history of the region more complicated. As the depth and seismic velocity properties of the LAB and MLD can reveal the spatial distributions of lithospheric deformation, destruction, and relevant tectonic processes, a deeper investigation of the LAB and MLD in the boundary region of NCC and XMOB will therefore provide seismic constraints on the mechanism of lithospheric modification and thinning, and important implications for the dynamics.

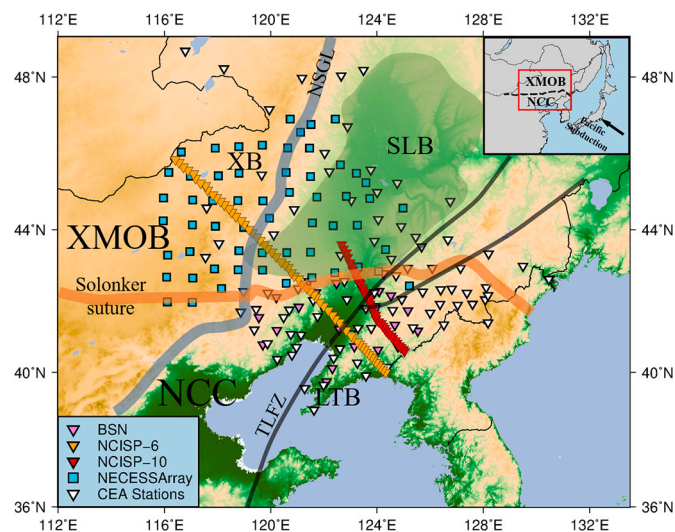


**Fig. 1.** Topographic map of the boundary region of NCC and XMOB showing the locations of stations used in this study. Tectonic blocks: NCC: North China Craton; XB: Xing'an block; SLB: Songliao Basin; LTB: Liaodong tectonic belt; NSGL: North-South Gravity Lineament; TLFZ: Tanlu Fault Zone. The light gray, light orange and dark gray dashed lines represent the locations of the NSGL, Solonker suture and TLFZ, respectively. The colored triangles are broadband seismic stations. The purple, yellow, red, and white triangles represent seismic array BSN, NCISP-6, NCISP-10, and CEA stations, respectively, while the cyan squares are the NECESSArray stations (the bottom left inset). The study region is outlined by a red rectangle in the upper right inset. The black arrow is the motion of the Paleo-Pacific plate subduction, and the black dashed lines represent the Solonker suture. (For interpretation of the references to colour in this figure legend, the reader is referred to the web version of this article.)

However, the seismic properties of the LAB and MLD in the boundary region of NCC and XMOB are not well studied. Previous studies on the seismic velocity structures in the boundary region of NCC and XMOB have mainly focused on the crustal structures (Wang et al., 2013; Tao et al., 2014; Zheng et al., 2015), the upper mantle discontinuities (Ai et al., 2003; Wang et al., 2013), and over-all tomographic velocity structures (Li and He, 2011; Guo et al., 2018). However, for the LAB, the previous studies are mainly focused on areas surrounding the boundary region of NCC and XMOB. For example, in the north of study region, the LAB in the middle part of the Xing'an block reaches a depth of 140–160 km, while that in the middle of the Songliao Basin is approximately at a depth of 100–120 km from the analysis of S-receiver functions (S-RFs) (Zhang et al., 2014). In the north of study region, especially the interior of the NCC, a high-resolution depth of the LAB, which ranges from 70 to >170 km, has been obtained from P-receiver functions (P-RFs) (Chen et al., 2006, 2008) and S-RF analysis (Chen et al., 2008, 2014; Zhang et al., 2019). In the boundary region of NCC and XMOB, the LAB depth was reported to be 100 km in the Liaodong tectonic belt and 140–160 km in the southern Xing'an block by using the depth of maximum velocity decreases obtained from inversion of surface waves (Li et al., 2011). However, surface waves are insensitive to velocity discontinuities, and surface waves cannot image the LAB depth with high resolution. Collectively, owing to the self-limitations of different methods and coverage of seismic data, these studies did not well resolve depth of the LAB in the boundary region of NCC and XMOB. Considering that a MLD of 80–110 km has been observed in the central and western parts of the NCC (Chen et al., 2014), whether a MLD exists in the interior of the lithosphere beneath the boundary region of NCC and XMOB is still unknown.

Here, we use the wave equation migration method for the S-RF (Chen et al., 2008) to investigate the high-resolution depth of the LAB and to verify the existence of the MLD in the boundary region of NCC and XMOB. S-RFs were calculated from waveform data of five seismic arrays deployed in the study region. The good coverage of the seismic stations allows us to obtain the spatial variations of the LAB depth and to determine the existence of the MLD. By combining the spatial variation in depth of the LAB and MLD in different tectonic blocks with geologic informatics, we can discuss the lithospheric deformation associated with Paleo-Pacific plate subduction.

## 2. Geological setting

The boundary region of NCC and XMOB includes the northern boundary of the NCC and southern XMOB, and these two blocks are separated by the Solonker suture zone. The NCC is one of the oldest cratons on Earth. As a whole, it was tectonically stable since its final cratonization in the late Paleoproterozoic. Since the Jurassic, the eastern NCC has undergone significant destruction and deformation. As a consequence, the ancient, cold, thin, and refractory craton-type lithospheric mantle in the eastern NCC was replaced by young, hot, thin, and relatively full oceanic-lithospheric mantle, accompanied by extensive magmatic activity, resulting in a significant increase in surface heat flow, large-scale structural extension and large basin formation (Xu, 2007). The deformation and destruction of the lithosphere in the NCC in the Phanerozoic not only obviously changed its internal tectonic pattern and lithospheric structure, but also inevitably left evolutionary imprints in the boundary regions. Previous studies on the lithospheric structure have covered almost all the regions of the NCC (Chen et al., 2006, 2008, 2014; Zhang et al., 2019, and references therein), except for the northern boundary of the NCC. In this study, using the seismic profiles traverse the northern boundary of the NCC and adjacent tectonic units, allows us to compare spatially uneven lithospheric deformation and thinning between the boundary region of NCC and XMOB and surrounding tectonic blocks.

The Xing-Meng Orogenic Belt, which belongs to the eastern part of the Central Asian Orogenic Belts (CAOB), has undergone multiple stages

of oceanic subduction, crustal accretion, collision and collage of different tectonic blocks, and post orogenic collapse and extension since the Early Paleozoic (Xiao et al., 2009). It is a giant accretionary orogenic belt with the longest developmental history and the most complicated magmatism. This complicated tectonic process must have left imprints on the lithospheric structure, especially the deformation and modification of the lithosphere. Studying the lithospheric structure of the region will thus provide seismic implications for regional tectonic evolution.

During the Mesozoic, the NCC and XMOB have been affected by the westward subduction of the Paleo-Pacific plate, which has subducted westward into the Northeastern Asia, and finally becomes stagnant in the Mantle Transition Zone (Zhu and Xu, 2019). The upper mantle above the stagnant slab was referred to as the Big Mantle Wedge (BMW) by Zhao et al., 2004 and Ohtani and Zhao, 2009. The BMW system is different from the conventional mantle wedge which is geographically close to the trench. Previous studies suggested the BMW was formed as early as in the early Cretaceous (Zhu et al., 2012; Ma and Xu, 2017; Xu et al., 2018). Mg isotope analyses on the continental basalts and circum-Pacific island arc basalts in the Late Mesozoic-Cenozoic indicates the influence of the BMW covers the NCC and XMOB (Li et al., 2017). Dehydration of the stagnant slab resulted in widespread volcanic activity (Wang et al., 2006; Ouyang et al., 2013; Xu et al., 2013a–c) in the eastern NCC during the Early Cretaceous. The partial melting within the BMW system exerted significant physio-chemical influence on the overlying lithospheric mantle, and might have played an important role in causing the lithosphere to thin and deform.

### 3. Data and method

#### 3.1. Data

Seismic data used in this study are mainly from five seismic arrays in the boundary region of NCC and XMOB, including the Northern China Interior Structure Project-6 [NCISP-6], the Northern China Interior Structure Project-10 [NCISP-10], the Bohaiwan Seismic Network [BSN], the NorthEast China Extended Seismic Array [NECESSArray], and the China Earthquake Administration [CEA]. The NCISP-6 operated from September 2008 to September 2009, starting from the Liaodong tectonic belt, crossing the southern Songliao Basin, and the southern Xing'an block, and ending at the border between China and Mongolia. Most of the stations were equipped with Guralp CMG-3ESP sensors (50 Hz to 30 s/60 s), a small number were CMG-3T sensors (50 Hz to 120 s), and the collectors were mainly REFTEK-130 and REFTEK-72A. The NCISP-10 operated from July 2016 to August 2018, crossed the Songliao Basin, and ended on the Liaodong tectonic belt. The instruments used were Guralp CMG-3ESP sensors (50 Hz to 30 s) and a REFTEK-130 collector. The BSN seismic array was planar with observations from May 2005 to May 2006. The Guralp CMG-3ESP sensors and REFTEK-72A digitizers were also used in the BSN array. The remaining two seismic array datasets are from the NECESSArray and China Earthquake Administration. The NECESSArray (Tao et al., 2014) was deployed in northeast China, with observation period from the September 2009 to August 2011. It consisted of 127 temporary broadband stations. Although the average station spacing is  $\sim 80$  km, which is too sparse to constrain the detailed lithosphere structure alone, we included the nearby NECESSArray stations to increase the coverage of the S-RF piercing points. The CEA stations were set up by the China Earthquake Administration as a part of the national seismic network. We only used data collected in the time period from October 2010 to December 2014 (Zheng et al., 2010). The seismometer misorientation of the stations was corrected. In total, data from 226 seismic stations (Fig. 1) were used to calculate the S-RFs.

#### 3.2. Method

With the advantage of separating S-p conversions from the multiples from the crust, the S-RFs have been widely used in imaging the LAB (P.

Kumar et al., 2005; Yuan et al., 2006; Chen et al., 2008). For S-RF calculation, we selected events (yellow dots in Fig. 2a) with the two principles (Yuan et al., 2006): a magnitude greater than 5.5 and an epicentral distance range of  $55^\circ$ – $85^\circ$ . Time-domain maximum entropy deconvolution (Wu and Zeng, 1998) was used to calculate S-RF. By comparing the signal to noise ratio of S-RF calculated with different Gaussian parameters, we selected a Gaussian parameter of 5 to ensure the resolution and a water level of 0.001 to suppress the noise. Finally, 4360 high-quality S-RFs were obtained from 226 seismic stations after careful visual inspection. The number of S-RFs obtained from NCISP-6 and NCISP-10 is dominant, as the two arrays followed a linear trend that traversed all major geologic blocks of study region with small station spacing. For most of the stations of the two arrays, the average number of S-RFs is larger than 30. While for the sporadic stations around these profiles (NECESSArray, BSN, CEA), the obtained S-RFs are about 20.

The wave equation post-stack depth migration (PSDM) method was used to obtain the detailed lithospheric structure (Chen et al., 2005). Compared with common conversion point (CCP) depth imaging (Zhu, 2000; Ai et al., 2003), the migration method improves the horizontal resolution, and helps to obtain a coherent structure beneath seismic stations. The practical application of the PSDM involves two steps: common conversion point (CCP) stacking (see in supplementary Fig. S1b) in the time domain, and backward wave field extrapolation in the frequency domain (Chen et al., 2008). For the CCP stacking, we first calculated the piercing points (blue, orange and green dots in Fig. 2c) of S-p conversions at different depths by using a modified 1-D IASP91 velocity model (Chen et al., 2006). Then, we designed the observing profiles (green solid lines in Fig. 2c) according to the distribution of piercing points. We set stacking bins at each depth along the profiles. The length of the bin was fixed at 160 km in the vertical direction of the profiles, while the width parallel to the profiles varied with the coverage of piercing points along the profiles. We followed the principles of ensuring that the minimum S-RF in each stacking bin were greater than 50. If the S-RF number was less than 50, the width of the stacking bin was broadened. Finally, we performed migration for S-RF as CCP gathers were got. To improve the signal-noise ratio, we ensured that the number of S-RF in each bin was greater than 50 (see in supplementary Fig. S1a) and set 0.01–0.50 Hz as the best frequency range (see in supplementary Fig. S3a, S3b).

According to the distributions of piercing points at depths of 100 km and 150 km, six observing profiles (green lines in Fig. 2c) were selected to construct the detailed depth of the LAB and MLD beneath the study area. Three of the profiles are in the NW-SE direction, while the other three are NE-SW oriented. The NW-SE profiles start from the Liaodong tectonic belt, across the Tanlu Fault Zone, the southern Songliao Basin, and southern Xing'an block, and end at the border between China and Mongolia. The NE-SW profiles are perpendicular to the former three profiles. Along the six observing profiles, we performed the post-stack migration method for S-RF. The CCP images are shown in the supplementary material, and migrated images of the six profiles are shown in Figs. 3 and 4. Furthermore, we present another S-RFs imaging profile parallel to the NCISP-10 seismic array (see in supplementary Fig. S4) for comparison with the NW-SE profiles.

### 4. The lithospheric structure beneath the boundary region of NCC and XMOB

#### 4.1. Determination of the MLD and LAB from the migrated images

In the migrated S-RF images, the consistent strong positive conversion phase at depths of 30–40 km is clearly identified as the Moho. Although it presents a relatively smooth feature, the depth of the Moho obviously deepens gradually from the southeastern Liaodong tectonic belt to the northwestern Xing'an block along the NW-SE profiles. The depth of the Moho is consistent with previous studies. The P-RF images

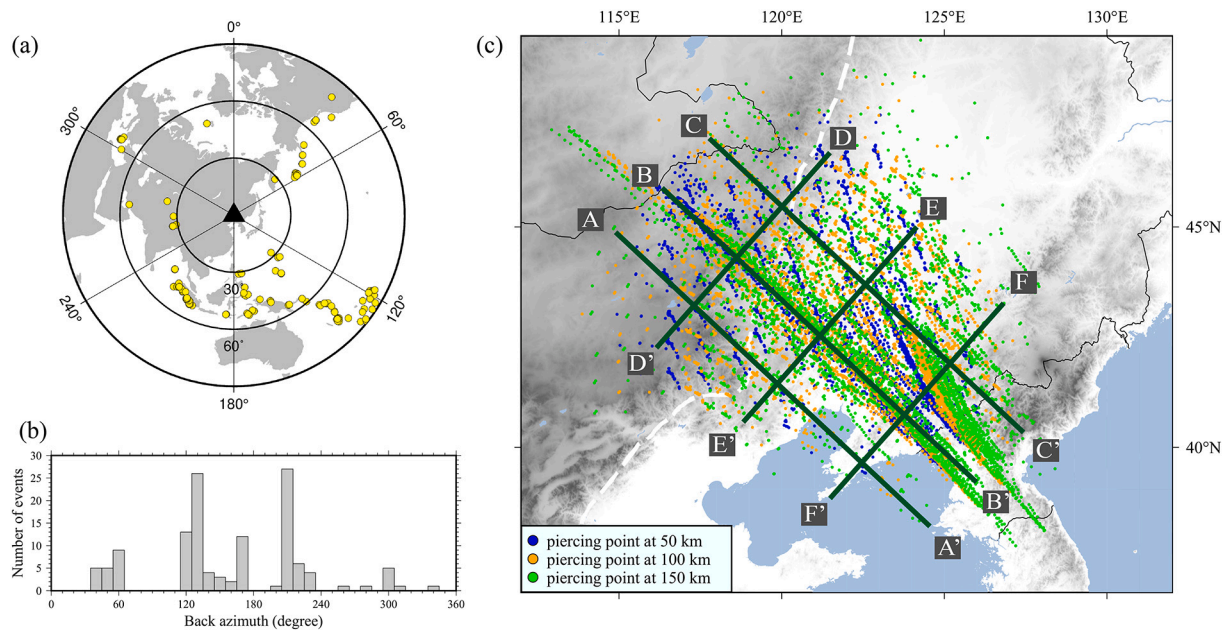


**Fig. 2.** (a) Distribution of the teleseismic events (yellow dots) used to calculate S-RFs. The black triangle is the location of the center of the study region. (b) Statistical histogram of the back azimuth of the events. Most events are located in the back azimuths of 120–180 and 200–230, while a small number of events are distributed in the back azimuths of 40–60 and 300. (c) Blue, orange and green dots represent the S-RF piercing points at 50 km, 100 km, and 150 km depths, respectively. The green solid lines represent different research profiles. The length of the three NW-SE profiles is 1000 km, while the three NE-SW profiles are 600 km. (For interpretation of the references to colour in this figure legend, the reader is referred to the web version of this article.)

show that the Moho depth in the southern Xing'an block is approximately 38 km, while the Moho depth in the Songliao Basin and Liaodong tectonic belt is much shallower (30–35 km) (Wang et al., 2013; Zheng et al., 2015). Moho depths measured by the H- $\beta$  and H-k methods also show the Moho in the southern Xing'an block is deeper than that in the Songliao Basin and its eastern flank (Tao et al., 2014), in consistent with our studies.

In addition to the Moho interface, there are two strong negative conversion phases (marked by white and red dashed lines) at depths of 60–100 km and 110–140 km shown in the migrated images (Fig. 3 and Fig. 4), respectively. As there is no strong negative conversion below the 110–140 km depth and in the consistency of migrated images with different frequencies (Fig. S3 in supplementary material), we interpret the strong negative conversion phase at depths of 110–140 km as the LAB. As a consequence, the negative conversion at depth of 60–100 km could be related to the S-p phase from the MLD. The migrated images for S-RF could be affected by many factors, including the data coverage, the signal-to-noise ratio, and lateral seismic heterogeneities. We have evaluated the robustness of the lithospheric discontinuities, by multi-frequency analysis, analyzing the data coverage at different depths (details in the supplementary material) and bootstrap (Efron, 1979) (Fig. S2 in supplementary material). Furthermore, we have evaluated the robustness of the lithospheric structural image by comparing the migrated images along different profiles (Fig. 4, and Fig. S4b in supplementary material). The consistency of negative phase depths (differently colored plus signals) among different profiles, reinforces that the negative phases at depths of 60–100 km and 110–140 km are the MLD and LAB, respectively.

#### 4.2. The variations in the depth of the MLD and LAB along the profiles

The three relatively NW-SE profiles reveal similar features of the MLD, although the three profiles are more than 100 km apart. Given the spatial distribution of the piercing points, the features of the MLD are more reliable along the distance of 200–950 km. The MLD presents an arc-shaped structure along the three long profiles. The shallowest MLD is found beneath the southern Songliao Basin at a depth of 60 km. The MLD

gradually deepens from the southern Songliao Basin to the western and eastern sides. The MLD reaches a depth of 100 km in the southern Xing'an block, while the depth of the MLD beneath the Tanlu Fault Zone and Liaodong tectonic belt is 70–80 km by contrast. The MLD beneath the three shorter NE-SW profiles shows different characteristics. The depth of the MLD deepens from 80 km in the western boundary of the Songliao Basin to a depth of 100 km in the southern Xing'an block along profile DD'. Migrated images of profiles EE' and FF' reveal a shallow MLD of 80 km beneath the southern Songliao Basin, the Tanlu Fault Zone, and the Liaodong tectonic belt.

As shown in Fig. 3, the depth of the LAB gradually deepens from southeast to northwest. In the southwest beneath the Xing'an block, a deeper LAB of 140 km is present, while the shallowest LAB of 110 km is present in the Tanlu Fault Zone and the Liaodong tectonic belt. The depth of the LAB in the southern Songliao Basin varies slightly from 110 to 130 km. S-p conversions from the LAB are incoherent along the profiles, which is different from features of the MLD. Especially in profile CC', there is a break in the LAB phase at a distance of 600–700 km. Additionally, the migrated images of profile AA' show similar characteristics. We speculate that the break in the LAB phase might be related to fewer S-RFs from the limited number of stations. As profile BB' contains more piercing points, the S-p phase from the LAB is relatively more consistent. Considering this, the LAB phase is weaker across ~600 km along profile BB'. The three short profiles have different trends compared with the long profiles. The LAB in the western boundary of the Songliao Basin reaches 120 km, while that beneath the southern Xing'an block is 140 km along profile DD'. In profile EE', there is a deep LAB of 140 km in the southern Songliao Basin, and a shallower LAB of 120 km at the northern boundary of the NCC, indicating the variation in the LAB depth between the XMOB and the northern boundary of NCC. The LAB phase shown in profile FF', which is almost in the northeastern NCC, reveals the shallowest LAB of 110 km in the study region. Furthermore, depth of MLD and LAB beneath the profile parallel to the NCISP-10 seismic array (see in supplementary Fig. S4) shows the same trend to that of profile BB'.

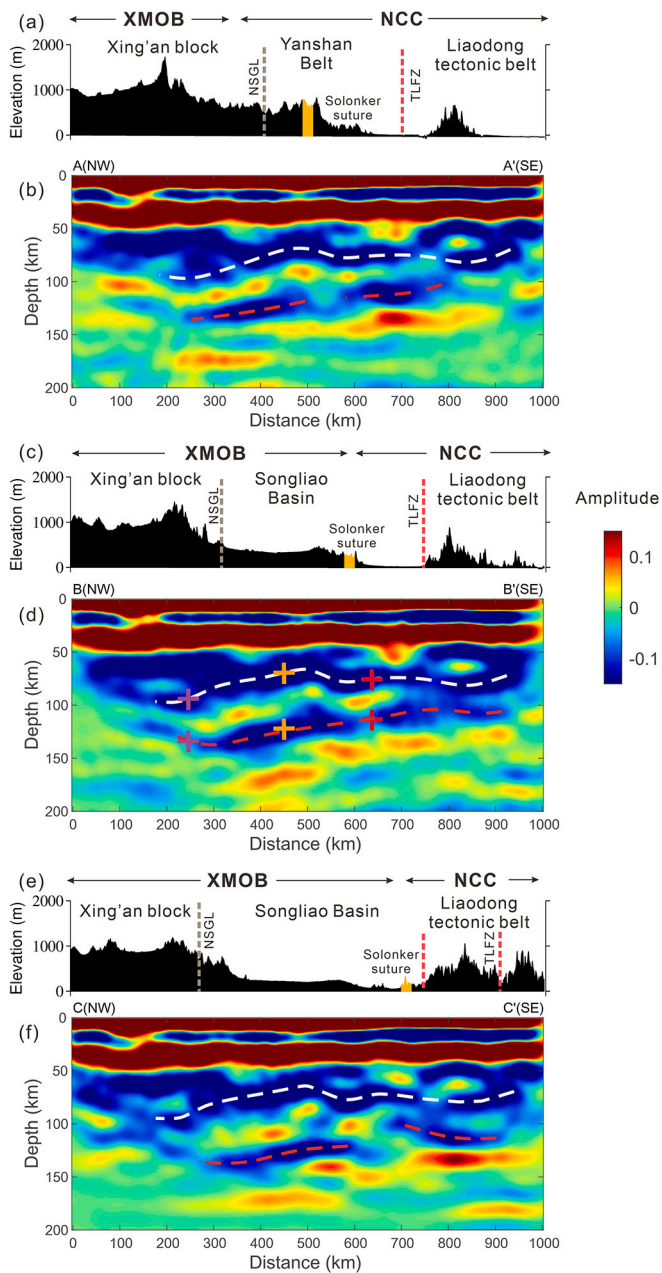


**Fig. 3.** S-RF migrated images of the three long profiles. (a), (c), and (e) show the surface topography of the three long profiles. The black arrows at the top are simple regional divisions of the Xing Meng Orogenic Belt (XMOB) and the North China Craton (NCC). The dark shaded areas indicate the elevation of the terrain. The vertical gray and red lines represent the NSGL and Tanlu Fault Zone, respectively. The vertical yellow rectangle is the location of Solonker suture. (b), (d), and (f) are the S-RF images that were constructed by using migration frequencies of 0.01–0.5 Hz. The negative phase in blue colour represents a velocity decrease with depth, while the positive phase with red colour represents a velocity increase with depth. The white and red dashed lines denote the MLD and LAB phases estimated by S-RFs, respectively. The differently colored plus signs in (d) are the coincidence of the long profiles and the relatively shorter profiles. (For interpretation of the references to colour in this figure legend, the reader is referred to the web version of this article.)

#### 4.3. Seismic properties (gradient thickness and velocity contrast) of the MLD and LAB

Analyzing the seismic properties, such as the gradient thickness and velocity contrast, of the velocity discontinuities (eg., MLD and LAB), can

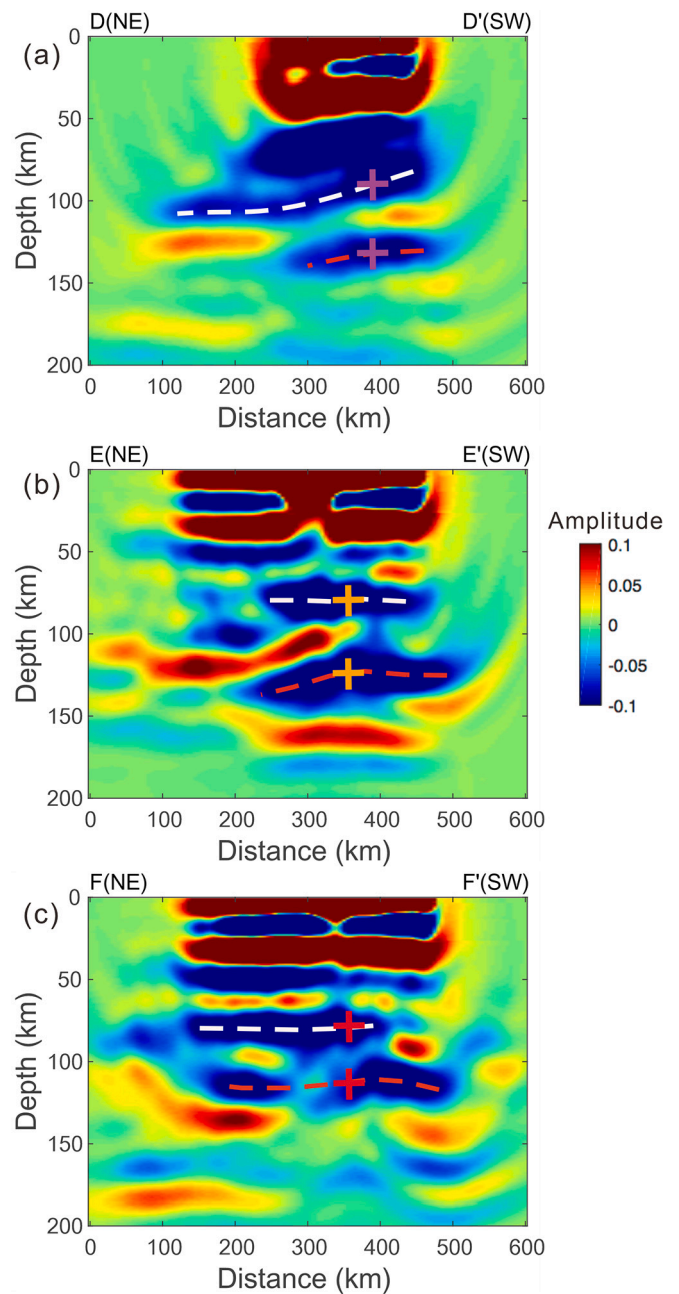


**Fig. 4.** S-RF migrated images of the three short profiles. The S-RF images were constructed by using migration frequencies of 0.01–0.5 Hz, which is the same as those used in the long profiles. The negative phase in blue colour represents a velocity decrease with depth, while the positive phase in red colour represents a velocity increase with depth. The white and red dashed lines denote the MLD and LAB phases estimated by S-RFs, respectively. The plus signs in the three figures are the coincidence locations of the long profiles and short profiles. And the differently colored plus signs correspond to that marked in Fig. 3.c. (For interpretation of the references to colour in this figure legend, the reader is referred to the web version of this article.)

provide implications for the dynamic formation process of velocity discontinuities. To analyze the properties of the MLD and LAB, a comparison between the observed CCP and the CCP images of synthetic S-RFs was carried out. Here, we performed the forward synthetic waveform by using the Raysum algorithm (Frederiksen and Bostock, 2000). The Raysum algorithm can generate sets of ray-theoretical seismograms for an incident plane wave (teleseismic approximation) for models consisting of a stack of layers. First, we selected one CCP stacking

waveform collected beneath the southern Songliao Basin, where the depth difference between the MLD and LAB is the largest. Second, we presented a 1-D velocity model incorporating the Moho, MLD, and LAB discontinuities and performed the Raysum algorithm to obtain the three components, and then we calculated the S-RF through time-domain maximum entropy deconvolution (Wu and Zeng, 1998). Additionally, head files of the observed S-RFs from four seismic stations close to the CCP stacking waveform were written to the forward synthetic S-RF. Finally, we constructed CCP stacking images for the synthetic seismograms in the same manner as the observing data. Fig. 5 shows the CCP stacking images of synthetic S-RFs calculated for different thickness of the velocity gradient and velocity contrast of the MLD (Fig. 5a) and LAB (Fig. 5b).

In Fig. 5a, velocity decreases of 4.5% (green dashed line) and 6.5% (blue dashed line) occurring over the gradient thickness of 0 km across the MLD show that the velocity contrast of 6.5% might only fit the amplitude of the real data but not the width. We selected a thickness of 10 km with different velocity contrasts of 6.5% (gray dashed line), 7.5% (black dashed line) and 8.5% (red dashed line). It could be seen that velocity decrease of 8.5% with a thickness of 10 km can best fit the real data. A sharp velocity decrease is also observed in other regions, such as the MLD in the Ontong Java Plateau with a velocity decrease of  $6 \pm 4\%$  (Tharimena et al., 2016). In the synthetic modeling of LAB (Fig. 5b), velocity decreases 6.5% (red dashed line) with a gradient thickness of 20 km are better able to match the real data. With the above comparison between the synthetic and the real data, the MLD and LAB present a different sharpness, although the two are both velocity decreasing discontinuities. Compared with the LAB, the MLD might be a relatively sharper discontinuity with a strong velocity contrast. The LAB with a relatively wider velocity gradient and lower velocity contrast, might be affected by the partial melting of the asthenosphere, meaning that there may have been destructive processes of the lithospheric mantle.

## 5. Discussion

### 5.1. The spatial variation in the depth of the MLD and its implications for the distribution of volcanism

According to the MLD depths obtained from the migrated images of the six observing profiles, the spatial distributions of the MLD depth (Fig. 6a) are obtained by using interpolation. The depth of the MLD trends from deep to shallow and from shallow to deep in the NW-SE direction (white arrows in Fig. 6a), forming an upward arc-shape in the southwestern Songliao Basin. The lateral variations in the MLD depth could be related to tectonic evolution, especially the Paleo-Pacific plate subduction since the Middle Mesozoic. With the continuous subduction of the Paleo-Pacific plate, and changes in the subduction angle, the boundary region of NCC and XMOB has undergone multiple stages of compression and extension (Zhu and Xu, 2019). The MLD thus deformed into an upward arc-shaped structure. The changing Paleo-Pacific plate subduction angle accompanied by retreat and rollback eventually led to stagnation of the Paleo-Pacific slab in the Mantle Transition Zone. Tectonic regime of the target region therefore changed from compression to extension. Volcanic activity, related to lithospheric extension, consequently occurred. Arc-shaped structure of the MLD might provide implications for the Cenozoic volcanoes distributed surrounding the Songliao Basin. Two-dimensional thermomechanical modeling of cratonic extension suggests that the MLD can enhance the deformation of the overlying mantle, suppress the deformation of underlying mantle, and resist hot materials from the asthenosphere (Liao and Gerya, 2014). In particular, there is a relatively deeper LAB beneath the arc-shaped MLD (comparison with the LAB in the Liaodong tectonic belt), formed a dense lower lithospheric mantle. The partially melting materials from the asthenosphere may thus be prevented from migrating to the surface within the Songliao Basin. The Cenozoic volcanic activities, such as the Abaga, Chifeng, and Changbai volcanoes, thus surround the Songliao Basin, and there is no volcanism within the basin.

Notably, migrated S-RFs images reveal an upward arc-shaped structure of MLD beneath the southwestern Songliao Basin, with the

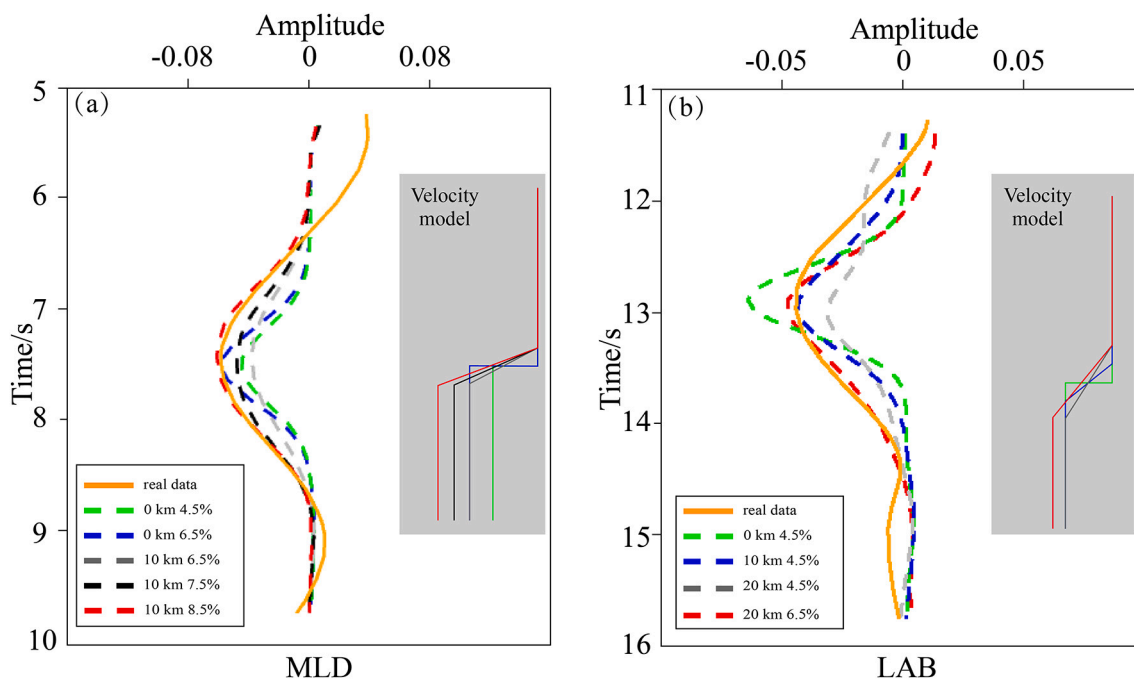
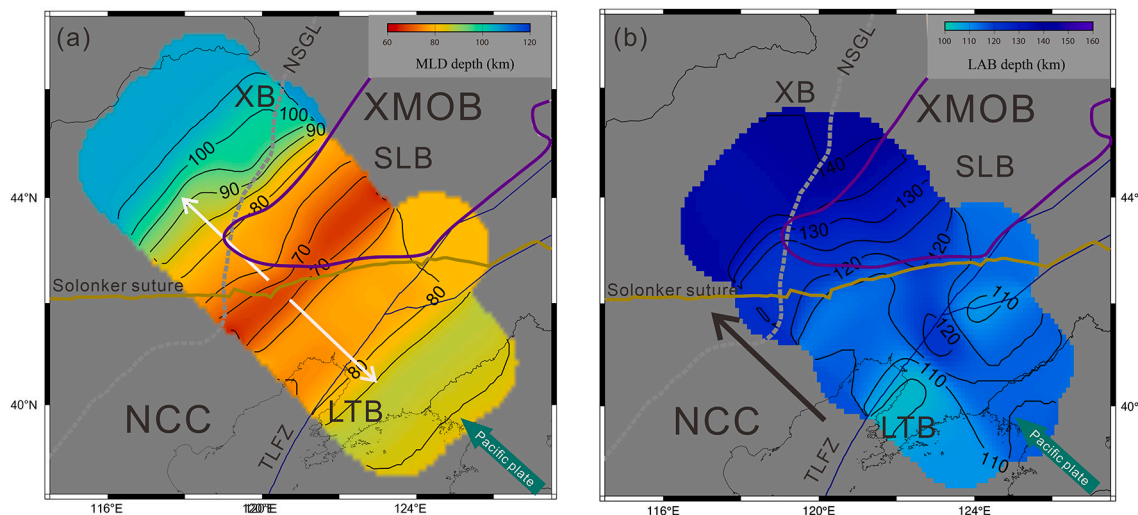


Fig. 5. Waveform comparisons between the observed receiver functions (yellow solid lines) and synthetic receiver functions (differently colored dashed lines). The input velocity models are given in the gray rectangular region. To obtain the obvious velocity contrast, we purely mark the velocity ratio  $(|V_{upper} - V_{lower}|) / V_{upper}$  at the velocity discontinuities (e.g., the MLD and LAB). (For interpretation of the references to colour in this figure legend, the reader is referred to the web version of this article.)



**Fig. 6.** The spatial variations in the MLD depth (a) and LAB depth (b) in the study region. Different colours correspond to distinct depths, and the corresponding values are given in the upper right corners. The black solid lines with numbers are the contours of the depth variations. The white and black arrows are the depth variations in the MLD and LAB, respectively. The purple solid lines represent the Songliao Basin. The light yellow solid lines represent the location of the Solonker suture, while the gray dashed lines indicate the NSGL. The green arrows are the direction of Paleo-Pacific plate subduction. (For interpretation of the references to colour in this figure legend, the reader is referred to the web version of this article.)

shallowest MLD located near the Solonker suture (Fig. 3). We suggest the shallowest MLD might be related to mantle melting (Liao and Gerya, 2014) due to decompression associated with the formation of Solonker suture. Numerous geological and geochemical studies suggested the Solonker suture was formed in the Late Triassic-Early Triassic, marking the northern boundary of the NCC, as well as the closure of the Paleo-Asian Ocean (Wang and Liu, 1986; Wang and Mo, 1995; Yin, 1996). Since the closure of the Paleo-Asian Ocean plate in the Middle Triassic (Xu et al., 2018), the Solonker suture zone entered post-orogenic extension (Xiao et al., 2003). After changing in the subduction direction of the Paleo-Pacific plate in the late Jurassic, the tectonic environment of the region finally became extensional, which resulted in the lithosphere modification and destruction, subsequently with mantle upwelling. The hot materials from mantle upwelling caused mantle melting along the MLD, resulting in the shallowest MLD. Furthermore, S-wave velocity structure from Rayleigh wave dispersion studies in the Solonker suture shows neglectable velocity contrast between the lithosphere and asthenosphere (Tang and Chen, 2008; Li and He, 2011), which means there might be metasomatism related to mantle upwelling in the transition zone of lithosphere and asthenosphere beneath the Solonker suture (Xu, 2007).

In addition to the spatial distribution of the MLD depth and the arc-shaped structure, the properties of the MLD, obtained from waveform modeling of synthetic S-RFs, show a sharp velocity decrease of 8.5% over <10 km. There are gradual and smooth temperature variations in the cratonic lithospheric mantle, resulting in gradual and smooth variations in the velocity of seismic waves. In comparison to the velocity decreases of 3% for MLDs in the Kalahari Craton (Sodoudi et al., 2013) and western United States (Lekić and Fischer, 2014), the properties of the MLD in the boundary region of NCC and XMOB cannot be explained purely by thermal mechanisms. As for the mechanism of the MLD is still debated, there are views explaining the existence of the MLD, such as the composition and radical anisotropy caused by metasomatic alteration, as well as partial melting and accretion of intrusive materials related to the formation of continents (Karato et al., 2015). Karato et al. (2015) suggested that the elastically accommodated grain-boundary sliding (EAGBS) model can also explain the mechanism of most MLDs distributed in different regions. Although there are many causes, in addition to the thermal activity, the sharper MLD may require a significant compositional change associated with partial melting within the

lithosphere.

Additionally, previous studies have suggested that a negative MLD phase is widely identified at depths of 80–110 km in the central and western parts of the NCC (Chen et al., 2014). It is worth noting that the MLD depth of 80–90 km obtained in our migrated images in the northeastern NCC is consistent with that in the central and western NCC. Furthermore, in contrast to the lithospheric structure images in the Tanlu Fault Zone along similar longitudes, the depth of MLD is 10–20 km deeper than the depth of the LAB in the Tanlu Fault Zone (Jiaodong Peninsula (Chen et al., 2006)). The existence of the MLD in the northeastern NCC therefore corroborates the speculation that the MLD has been existed beneath the eastern NCC before its destruction in the Mesozoic (Chen et al., 2014). Alkaline magmatism, such as syenites, was distributed in the eastern NCC in the Paleozoic to early Mesozoic. Element composition of the alkaline rocks indicates that they were derived from the enriched, refractory lithospheric mantle (Yang et al., 2012). Previous studies suggested metasomatically enriched components could be found at depth of 100 km in the continental lithospheric mantle (O'Reilly and Griffin, 2010). Thus, alkaline magmatism provides evidence for the existence of metasomatism or a MLD probably within the lithosphere in the eastern NCC before its destruction in Mesozoic (Chen et al., 2014).

Together with the spatial distribution of the MLD in the central and western NCC, the lithospheric deformation and modification in the northeastern NCC might be more localized than that in Tanlu Fault Zone, and especially influenced by Paleo-Pacific plate subduction in the Mesozoic. Additionally, the trend of the variation in the MLD depth is parallel to the direction of Paleo-Pacific plate subduction (green arrows in Fig. 6a), which might reveal the influence of Paleo-Pacific plate subduction. In contrast to the shallowest MLD in the southern Songliao Basin, the relatively deeper MLD in the southern Xing'an block further indicates that the influence of Paleo-Pacific plate subduction may weaken near the NSGL.

## 5.2. The spatial variation in the depth of the LAB and its implications for lithospheric deformation and thinning

Different from the depth of the MLD, the depth of the LAB in the region shows a general tendency of NW-ward deepening (black arrows in Fig. 6b). The LAB also displays different characteristics between the

northeastern NCC (including the Tanlu Fault Zone and Liaodong tectonic belt) and the southern XMOB. The LAB is shallowest at depths of 105–120 km around the Liaodong tectonic belt and Tanlu Fault Zone, while the LAB reaches a depth of 140 km in the southern Xing'an block. In addition to the deepening trend from SE to NW, the LAB depth also shows variation along the S–N direction in the northern boundary of the NCC. The LAB is shallower within the NCC, at depth of 110 km, while that in the southern Songliao Basin reaches a depth of 130 km.

The spatial variations in the LAB depth show consistent features with previous studies using different methods and data in the boundary region of NCC and XMOB. The S-wave velocity structure of the lithosphere obtained from Rayleigh wave topographic measurements shows strong lateral heterogeneity (Li and He, 2011). The depth of LAB, estimated from the depth of the maximum velocity decrease, reaches 100 km in the Liaodong tectonic belt and 120–150 km in the southern Xing'an block. Given the depth uncertainties from two studies (Fischer et al., 2010), there is a good agreement between the LAB depth estimated from the Rayleigh wave and our migrated images. By using the seismic data from the interior of NCC, Chen et al., 2008 suggested that the LAB in the southern Songliao Basin and Tanlu Fault Zone could reach depth of over ~100 km. Zhang et al., 2014 further identified the LAB at depths of 140–160 km in the Xing'an block and at a depth of 100–120 km in the Songliao Basin, which is consistent with the LAB depth in our results. The variation of the LAB depth obtained in our results also coincides with the observation of locally low surface heat flux in the northern boundary of the NCC (Hu et al., 2000). Indeed, the agreement among different reinforces the robustness of the LAB depth beneath the study region obtained in our study.

Studies of xenoliths in kimberlites indicate that there was a thick lithosphere of ~180 km in the Paleozoic (Menzies et al., 1993; Griffin et al., 1998) beneath the NCC. Even considering the vertical resolution in the S-RF migration images, the estimated depth of the LAB in the northeastern NCC never reaches 140 km. The LAB depth estimated in our S-RF migrated images provides seismic evidence for the occurrence of significant lithospheric modification and thinning in the northeastern NCC since the Phanerozoic. Moreover, lithospheric modification and thinning show the characteristics of spatial lateral inhomogeneity among the different tectonic blocks in the study region. Particularly in the southern Xing'an block with a relatively deeper LAB of 140 km. Although depth of the LAB in the Xing'an block is unknown before the Paleo-Pacific plate subduction, the lithosphere modification and thinning process probably were weakening due to its location far from the Paleo-Pacific plate. The depth changes of the LAB outside and inside part of the NCC, together with significantly different fast directions and large delay times obtained from SKS splitting measurements across the northern boundary of the NCC (Zhao et al., 2007), indicate a different deformation mechanism of the upper mantle. Additionally, our S-RF migrated images corroborate the speculation that the rapid variation in upper mantle anisotropy was caused by lateral variations in the LAB depth (Zhao and Zheng, 2007). Furthermore, Previous studies (Xu, 2001; Zheng et al., 1998; Xu et al., 2004) suggest the Tanlu Fault Zone, which is major active strike-slip fault zone in eastern China, might be the main factor for the lithosphere thinning in the eastern NCC since the Mesozoic. Notably, the LAB is about the shallowest along the Tanlu Fault Zone in the migrated images. Combining with the LAB depth of 60–70 km in the Jiaodong Peninsula (Chen et al., 2006), we speculate the Tanlu Fault Zone might play a significant role in the lithosphere extension and thinning in the eastern NCC. Moreover, the shallowest LAB in the Tanlu Fault Zone provides the speculation that the Tanlu Fault Zone might be a lithosphere-scale fault system (Zheng et al., 2008).

How did the lithosphere in the study region be modified and thinned? Notably, the spatial variation in the LAB depth is consistent overall with the Paleo-Pacific plate subduction. Numerous studies from the tomography images (Zhao et al., 2004; Huang and Zhao, 2006; Ohtani and Zhao, 2009) show the existence of the stagnant Pacific slab in the Xing-Meng Orogenic Belt. Liu et al. (2017) suggested the existence of a

flat slab in the Mantle Transition Zone is no more than 20 million years by using high-resolution model of P-wave tomography and paleo-age data of ancient seafloor. Although the observed BMW system by tomography was formed in the Cenozoic, Zhu et al. (2012) suggest the BMW have been formed since the early Cretaceous with the subduction of Paleo-Pacific plate. Since the lithosphere in the eastern NCC was destroyed in the Mesozoic (e.g. Chen et al., 2008; Zhu and Zheng, 2009), combining with the spatial variation in the LAB depth, we speculate that the subduction of Paleo-Pacific plate is the dominant factor controlling the dynamic process of the boundary region of NCC, XMOB and adjacent regions since the early Cretaceous (Zheng and Wu, 2009). Therefore, the lithospheric modification and thinning in the study region might be related to the BMW associated with the stagnant Paleo-Pacific slab. Significant amounts of water and carbonatite melts released by the dehydration of the stagnant Paleo-Pacific slab within the Mantle Transition Zone (Xu et al., 2018; Xia et al., 2019; Li and Wang, 2018) lead to the partial melting of the BMW and upward migration of the deep fluids into the shallow lithospheric mantle (Fig. 7). The lithospheric mantle is hydrated and unsteady, resulting in an increase in hot fluids and melts in the overlying lithospheric mantle, and consequently with an increase in the lithospheric extension and thermal anomalies. Collectively, the physical and chemical properties of the lithospheric mantle have therefore significantly changed, and it manifests as lithospheric modification and thinning in the boundary region of NCC and XMOB. Moreover, before lithospheric extension in the Late Mesozoic, there were several phases of compressive deformation in the N-S direction at the northern boundary of the NCC (Meng, 2003). The N-S directed variation in the LAB depth across the northern boundary of the NCC might preserve the trace of compressive deformation.

Significant changes in the physical and chemical properties of the lithospheric mantle certainly have redefined the boundary region between the lithosphere and asthenosphere, that is, the LAB. In addition to the significant thinning of the lithosphere, the boundary region of NCC and XMOB is characterized by a relatively sharp LAB at present. As previously discussed in Section 4.3, waveform forward modeling of S-RFs showed a strong, sharp velocity decrease (7.5–8.5% over <10 km) in the MLD, and a relatively weaker velocity decrease (6.5% over <20 km) in the LAB in the study region. Geodynamic models for cratonic lithosphere suggest that the sharper LAB cannot be explained by temperature alone (King and Ritsema, 2000; King and Jordan, 2002; Cooper et al., 2004). Even considering the uncertainties in the estimated LAB depth, the velocity gradient of the LAB in the study region is at least less than 20–30 km. We thus conclude that such velocity gradients of the LAB in the study region cannot be explained purely by an increase in temperature from the lithosphere to the asthenosphere. The sharpness of the LAB indicates there must be an additional property or process in addition to temperature to explain the velocity gradient. One possible cause for the velocity decrease of the relatively sharper LAB is that there is a more dehydrated lithosphere in contrast to hydrated and fertile asthenosphere (Karato and Jung, 1998). Studies on the Phanerozoic Australian lithosphere show that the depletion alone could cause a velocity decrease of no more than 1% or so (Lee, 2003) and hydration of the asthenosphere could reduce velocity decrease of approximately 4.5% (Rychert and Shearer, 2009).

Alternatively, a large velocity decrease could be produced by a small amount of partial melting (Rychert et al., 2005, 2007; Tharimena et al., 2017) in the asthenosphere. Previous studies have shown that the S wave velocity reduction per percent partial melt could reach at least 7.9% (Hammond and Humphreys, 2000). The large and rapid velocity decrease of the LAB in western America has been proven to be associated with the increased water content in the partial melting and anomalously hot asthenosphere (Foster et al., 2014). Kawakatsu et al. (2009) also showed a partial melting beneath the Pacific Plate descending beneath Japan based on receiver function imaging. As partial melting might exist beneath hot spots and subduction zones, we suggest that the sharp LAB in the boundary region of NCC and XMOB can be explained by partial

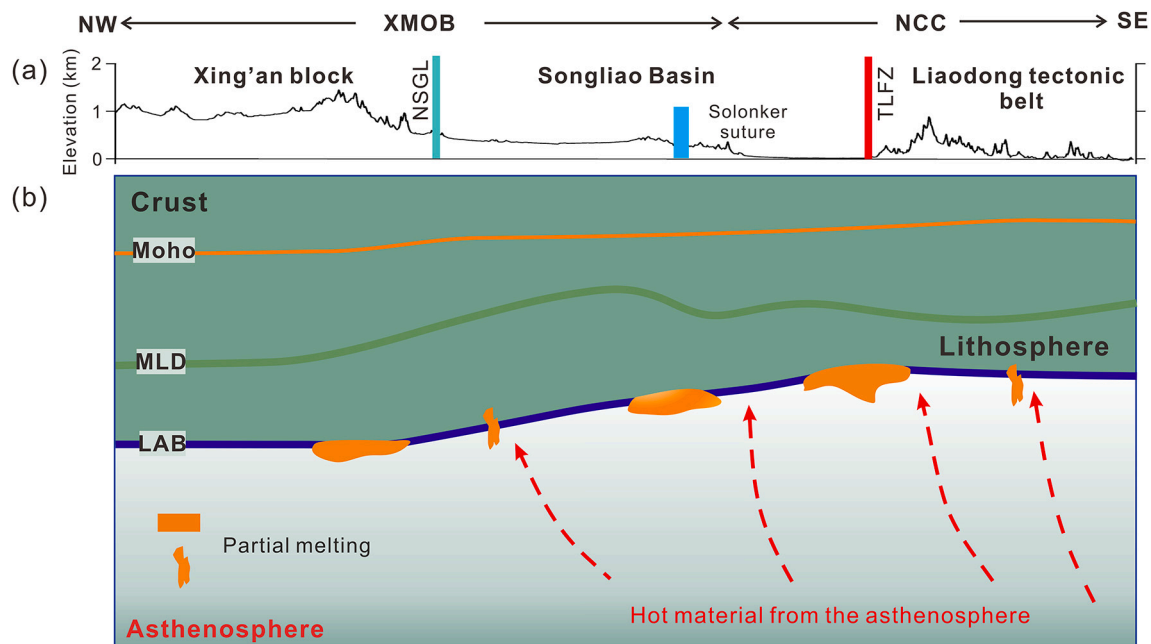


**Fig. 7.** Schematic cartoon explaining the tectonic evolution of the study region (the lithospheric structure is from the migrated image of profile BB'). (a) Topography of the study region. The black arrows at the top are simple regional divisions of the Xing Meng Orogenic Belt (XMOB) and the North China Craton (NCC). The cyan, blue and red vertical solid lines are the NSGL, Solonker suture and TLFZ, respectively. (b) The orange and green solid lines are the locations of the Moho and MLD, respectively, while the blue solid line indicates the depth of the LAB. The yellow lumps surrounding the LAB are partial melting related to hot material from the asthenosphere, which directly resulted in the destruction of the lithosphere in the study region. The red dashed arrows indicate the hot material from the asthenosphere associated with the Big Mantle Wedge, which is related to Paleo-Pacific plate subduction and its stagnation in the mantle transition zone. (For interpretation of the references to colour in this figure legend, the reader is referred to the web version of this article.)

melting due to the dehydration of the Paleo-Pacific slab (Fig. 7). Carbonatite melts and significant amounts of water in the BMW could lower the melting temperature and facilitates partial melting (Fig. 7). As a result, the physical and chemical properties of the lithospheric mantle would be significantly changed, consequently with lithospheric modification and thinning.

## 6. Conclusions

By using S receiver functions (S-RFs) calculated from high quality broadband seismic data, depths of the lithosphere–asthenosphere boundary (LAB) and mid-lithosphere discontinuity (MLD) beneath the boundary region of North China Craton (NCC) and Xing Meng Orogenic Belt (XMOB) are well imaged. The following new insights are gained from the depth variations and properties of the LAB and MLD:

- (1) In contrast to the LAB of  $\sim >180$  km estimated from xenoliths in kimberlites in the Paleozoic, the depth of the present LAB indicates inhomogeneous lithospheric deformation and thinning in the northeastern NCC, especially significant diverse lithospheric thinning between the northeastern NCC and the adjacent southern XMOB.
- (2) A coherent MLD is identified beneath the boundary region of NCC and XMOB, indicating strong lithospheric layering in the target region. The MLD also provides seismic evidence for the speculation that the MLD existed in the eastern NCC before its destruction in the Mesozoic. Furthermore, the existence of the MLD in the northeastern NCC reveals spatially uneven lithospheric destruction in different parts of the eastern NCC.
- (3) The seismic properties of the LAB and MLD indicate that lithospheric deformation and thinning might be related to the partial melting induced by the Big Mantle Wedge associated with the subducting Paleo-Pacific plate and its stagnation during the Late Mesozoic. Such partial melting efficiently reduces the S wave

velocity and could well explain the sharp LAB phases reported in our migrated images.

## Declaration of Competing Interest

The authors declare that they have no known competing financial interests or personal relationships that could have appeared to influence the work reported in this paper.

## Acknowledgements

We shall extend our thanks to the Seismic Array Laboratory of IGGCAS for providing the waveform data (doi:10.12129/IGGSL.Data.Observation). We also thank the Data Management Center of China National Seismic Network at Institute of Geophysics, China Earthquake Administration for the data from the permanent stations (SEISDMC; doi:10.11998/seisdmc/SN). The NECESSArray data are provided by IRIS Data Management Center (<http://ds.iris.edu>). Figures are generated by the Generic Mapping Tools (GMT) (Wessel et al., 2013). This study is supported by the National Key R&D Program of China (Grant No.2016YFC 0600101) and the Strategic Priority Research Program (B) of Chinese Academy of Sciences (Grant XDB18000000).

## Appendix A. Supplementary data

Supplementary data to this article can be found online at <https://doi.org/10.1016/j.tecto.2021.229067>.

## References

- Abt, D.L., Fischer, K.M., French, S.W., Ford, H.A., Yuan, H.Y., Romanowicz, B., 2010. North American lithospheric discontinuity structure imaged by Ps and Sp receiver functions. *J. Geophys. Res. Solid Earth* 115, B09301. <https://doi.org/10.1029/2009JB006914>.

- Ai, Y., Zheng, T., Y., 2003. The upper mantle discontinuity structure beneath eastern China. *Geophys. Res. Lett.* 30 (20).
- Chen, L., Wen, L., Zheng, T., 2005. A wave equation migration method for receiver function imaging. *J. Geophys. Res. Solid Earth* 110, B11309.
- Chen, L., Zheng, T., Xu, W., 2006. A thinned lithospheric image of the Tanlu Fault Zone, eastern China: constructed from wave equation-based receiver function migration. *J. Geophys. Res. Solid Earth* 111, B09312.
- Chen, L., Tao, W., Zhao, L., Zheng, T., 2008. Distinct lateral variation of lithospheric thickness in the Northeastern North China Craton. *Earth Planet. Sci. Lett.* 267 (1–2), 56–68.
- Chen, L., Jiang, M., Yang, J., Wei, Z., Liu, C., Ling, Y., 2014. Presence of an intralithospheric discontinuity in the central and western North China Craton: implications for destruction of the craton. *Geology* 42 (3), 223–226.
- Cooper, C.M., Lenardic, A., Moresi, L., 2004. The thermal structure of stable continental lithosphere within a dynamic mantle. *Earth Planet. Sci. Lett.* 222 (3–4), 807–817.
- Efron, B., 1979. Bootstrap methods: another look at the Jackknife. *Ann. Stat.* 1–26.
- Fischer, K.M., Ford, H.A., Abt, D.L., Rychert, C.A., 2010. The lithosphere-asthenosphere boundary. *Annu. Rev. Earth Planet. Sci.* 38, 551–575.
- Ford, H.A., Fischer, K.M., Abt, D.L., Rychert, C.A., Elkins-Tanton, L.T., 2010. The lithosphere-asthenosphere boundary and cratonic lithospheric layering beneath Australia from s-p wave imaging. *Earth Planet. Sci. Lett.* 300 (3–4), 299–310.
- Foster, K., Dueker, K., Schmandt, B., Yuan, H., 2014. A sharp cratonic lithosphere-asthenosphere boundary beneath the American Midwest and its relation to mantle flow. *Earth Planet. Sci. Lett.* 402, 82–89.
- Frederiksen, A.W., Bostock, M.G., 2000. Modelling teleseismic waves in dipping anisotropic structures. *Geophys. J. Int.* 141 (2), 401–412.
- Griffin, W.L., Andi, Z., O'reilly, S.Y., Ryan, C.G., 1998. Phanerozoic evolution of the lithosphere beneath the Sino-Korean Craton. In: *Mantle dynamics and plate interactions in East Asia*, 27, pp. 107–126.
- Guo, Z., Wang, K., Yang, Y., Tang, Y., John Chen, Y., Hung, S.H., 2018. The origin and mantle dynamics of quaternary intraplate volcanism in Northeast China from joint inversion of surface wave and body wave. *J. Geophys. Res. Solid Earth* 123 (3), 2410–2425.
- Hammond, W.C., Humphreys, E.D., 2000. Upper mantle seismic wave velocity: Effects of realistic partial melt geometries. *J. Geophys. Res. Solid Earth* 105 (B5), 10975–10986.
- Hönik, T., Lenardic, A., 2010. Long wavelength convection, Poiseuille–Couette flow in the low-viscosity asthenosphere and the strength of plate margins. *Geophys. J. Int.* 180 (1), 23–33.
- Hu, S., He, L., Wang, J., 2000. Heat flow in the continental area of China: a new data set. *Earth Planet. Sci. Lett.* 179 (2), 419.
- Huang, J., Zhao, D., 2006. High-resolution mantle tomography of China and surrounding regions. *J. Geophys. Res. Solid Earth* 111 (B9).
- Karato, S.I., Jung, H., 1998. Water, partial melting and the origin of the seismic low velocity and high attenuation zone in the upper mantle. *Earth Planet. Sci. Lett.* 157 (3–4), 193–207.
- Karato, S.I., Olugboji, T., Park, J., 2015. Mechanisms and geologic significance of the mid-lithosphere discontinuity in the continents. *Nat. Geosci.* 8 (7), 509–514.
- Kawakatsu, H., Kumar, P., Takei, Y., Shinohara, M., Kanazawa, T., Araki, E., Suyehiro, K., 2009. Seismic evidence for sharp lithosphere-asthenosphere boundaries of oceanic plates. *Science* 324 (5926), 499–502.
- King, S.D., Ritsema, J., 2000. African hot spot volcanism: small-scale convection in the upper mantle beneath cratons. *Science* 290 (5494), 1137–1140.
- Kumar, P., Yuan, X., Kind, R., Kosarev, G., 2005. The lithosphere-asthenosphere boundary in the Tien Shan-Karakoram region from S receiver functions: evidence for continental subduction. *Geophys. Res. Lett.* 32 (7), L07305.
- Lee, C.T.A., 2003. Compositional variation of density and seismic velocities in natural peridotites at STP conditions: implications for seismic imaging of compositional heterogeneities in the upper mantle. *J. Geophys. Res. Solid Earth* 108 (B9).
- Lekić, V., Fischer, K.M., 2014. Contrasting lithospheric signatures across the western United States revealed by Sp receiver functions. *Earth Planet. Sci. Lett.* 402, 90–98.
- Li, M., He, Y., 2011. Lithospheric structure beneath northeastern boundary region of the North China Craton from Rayleigh wave dispersion inversion. *Acta Seismol. Sin.* 33 (2), 143–155.
- Li, S., Wang, Y., 2018. Formation time of the big mantle wedge beneath eastern China and a new lithospheric thinning mechanism of the North China craton—Geodynamic effects of deep recycled carbon. *Sci. China Earth Sci.* 61 (7), 853–868.
- Li, S.G., Yang, W., Ke, S., Meng, X.N., Tian, H.C., Xu, L.J., He, Y.S., Huang, J., Wang, X.C., Xia, Q.K., Sun, W.D., Yang, X.Y., Ren, Z.Y., Wei, H.Q., Liu, Y.S., Meng, F.C., Yan, J., 2017. Deep carbon cycles constrained by a large-scale mantle Mg isotope anomaly in eastern China. *Natl. Sci. Rev.* 298, 111–120.
- Liao, J., Gerya, T., 2014. Influence of lithospheric mantle stratification on craton extension: insight from two-dimensional thermo-mechanical modeling. *Tectonophysics* 631, 50–64.
- Liu, X., Zhao, D., Li, S., Wei, W., 2017. Age of the subducting Pacific slab beneath east Asia and its geodynamic implications. *Earth Planet. Sci. Lett.* 464, 166–174.
- Ma, Q., Xu, Y.G., 2017. The temporal and spatial changes of Mesozoic magma in the East Asia and the formation time of the big mantle wedge. In: *Annual Meeting of Chinese Geoscience Union*.
- Meng, Q.R., 2003. What drove late Mesozoic extension of the northern China–Mongolia tract? *Tectonophysics* 369, 155–174.
- Menzies, M.A., Fan, W., Zhang, M., 1993. Palaeozoic and Cenozoic lithoprobes and the loss of >120 km of Archaean lithosphere, Sino-Korean craton, China. *Geol. Soc. Lond., Spec. Publ.* 76 (1), 71–81.
- Ohtani, E., Zhao, D., 2009. The role of water in the deep upper mantle and transition zone: dehydration of stagnation slabs and its effects on the big mantle wedge. *Russ. Geol. Geophys.* 50 (12), 1073–1078.
- O'Reilly, S.Y., Griffin, W.L., 2010. The continental lithosphere–asthenosphere boundary: can we sample it? *Lithos* 120 (1–2), 1–13.
- Ouyang, H.G., Mao, J.W., Santosh, M., Zhou, J., Zhou, Z.H., Wu, Y., Hou, L., 2013. Geodynamic setting of Mesozoic magmatism in NE China and surrounding regions: perspectives from spatio-temporal distribution patterns of ore deposits. *J. Asian Earth Sci.* 78, 222–236.
- Rychert, C.A., Shearer, P.M., 2009. A global view of the lithosphere-asthenosphere boundary. *Science* 324 (5926), 495–498.
- Rychert, C.A., Fischer, K.M., Rondenay, S., 2005. A sharp lithosphere–asthenosphere boundary imaged beneath eastern North America. *Nature* 436 (7050), 542–545.
- Rychert, C.A., Rondenay, S., Fischer, K.M., 2007. P-to-S and S-to-P imaging of a sharp lithosphere-asthenosphere boundary beneath eastern North America. *J. Geophys. Res. Solid Earth* 112 (B8).
- Selway, K., Ford, H., Kelemen, P., 2015. The seismic mid-lithosphere discontinuity. *Earth Planet. Sci. Lett.* 414, 45–57.
- Sodoudi, F., Yuan, X., Kind, R., Lebedev, S., Adam, J.M.C., Kästle, E., Tilmann, F., 2013. Seismic evidence for stratification in composition and anisotropic fabric within the thick lithosphere of Kalahari Craton. *Geochem. Geophys. Geosyst.* 14 (12), 5393–5412.
- Tang, Q., Chen, L., 2008. Structure of the crust and uppermost mantle of the Yanshan Belt and adjacent regions at the northeastern boundary of the North China Craton from Rayleigh wave dispersion analysis. *Tectonophysics* 455 (1–4), 43–52.
- Tang, J., Xu, W., Wang, F., Ge, W., 2018. Subduction history of the Paleo-Pacific slab beneath Eurasian continent: Mesozoic–Paleogene magmatic records in Northeast Asia. *Sci. China Earth Sci.* 61 (5), 527–559.
- Tao, K., Niu, F., Ning, J., Chen, Y.J., Grand, S., Kawakatsu, H., Ni, J., 2014. Crustal structure beneath NE China imaged by NECESSArray receiver function data. *Earth Planet. Sci. Lett.* 398, 48–57.
- Tharimena, S., Rychert, C.A., Harmon, N., 2016. Seismic imaging of a mid-lithospheric discontinuity beneath Ontong Java Plateau. *Earth Planet. Sci. Lett.* 450, 62–70.
- Tharimena, S., Rychert, C., Harmon, N., 2017. A unified continental thickness from seismology and diamonds suggests a melt-defined plate. *Science* 357 (6351), 580–583.
- Wang, Q., Liu, X., 1986. Paleoplate tectonics between cathaysia and angaraland in Inner Mongolia of China. *Tectonics* 5 (7), 1073–1088.
- Wang, H.Z., Mo, X.X., 1995. An outline of the tectonic evolution of China. *Episodes* 18 (1), 6–16.
- Wang, F., Zhou, X.H., Zhang, L.C., Ying, J.F., Zhang, Y.T., Wu, F.Y., Zhu, R.X., 2006. Late Mesozoic volcanism in the Xing'an block (NE China): timing and implications for the dynamic setting of NE Asia. *Earth Planet. Sci. Lett.* 251 (1–2), 179–198.
- Wang, B., Chen, L., Ai, Y., 2013. Crustal structure and mantle transition zone thickness beneath the northeastern area of the North China Craton and adjacent region. *Chin. J. Geophys. (in Chinese)* 56 (1), 60–68.
- Wang, T., Zhang, L., Guo, L., Wang, X.X., Li, S., Feng, C.Y., Zhang, C.L., 2014. The progress of the preliminary compilation of map of Mesozoic Cratoid of Asia and research on related key issues. *Acta Geosci. Sin.* 35 (6), 655–672.
- Wessel, P., Smith, W.H.F., Scharroo, R., Luis, J., Wobbe, F., 2013. Generic mapping tools: improved version released. *Eos, Trans. Am. Geophys. Union* 94 (45). <https://doi.org/10.1002/2013EO450001>.
- Wu, Q., Zeng, R., 1998. The crustal structure of Qinghai-Xizang plateau inferred from broadband teleseismic waveform. *Acta Geophys. Sin.* 41 (5), 669–679.
- Xia, Q.K., Liu, J., Kovács, I., Hao, Y.T., Li, P., Yang, X.Z., Sheng, Y.M., 2019. Water in the upper mantle and deep crust of eastern China: concentration, distribution and implications. *Natl. Sci. Rev.* 6 (1), 125–144.
- Xiao, W., Windley, B.F., Hao, J., Zhai, M., 2003. Accretion leading to collision and the Permian Solonker suture, Inner Mongolia, China: termination of the central Asian orogenic belt. *Tectonics* 22 (6).
- Xiao, W.J., Windley, B.F., Huang, B.C., Han, C.M., Yuan, C., Chen, H.L., Li, J.L., 2009. End-Permian to mid-Triassic termination of the accretionary processes of the southern Altaids: implications for the geodynamic evolution, Phanerozoic continental growth, and metallogeny of Central Asia. *Int. J. Earth Sci.* 98 (6), 1189–1217.
- Xu, Y.G., 2001. Thermo-tectonic destruction of the Archaean lithospheric keel beneath the Sino-Korean Craton in China: evidence, timing and mechanism. *Phys. Chem. Earth Solid Earth Geod.* 26 (9–10), 747–757.
- Xu, Y.G., 2007. Diachronous lithospheric thinning of the North China craton and formation of the Daxin'anling–Taihangshan gravity lineament. *Lithos* 96 (1–2), 281–298.
- Xu, Y.G., Chung, S.L., Ma, J., Shi, L., 2004. Contrasting Cenozoic lithospheric evolution and architecture in the western and eastern Sino-Korean Craton: constraints from geochemistry of basalts and mantle xenoliths. *J. Geol.* 112 (5), 593–605.
- Xu, W.L., Pei, F.P., Wang, F., Meng, E., Ji, W.Q., Yang, D.B., Wang, W., 2013a. Spatial–temporal relationships of Mesozoic volcanic rocks in NE China: constraints on tectonic overprinting and transformations between multiple tectonic regimes. *J. Asian Earth Sci.* 74, 167–193.
- Xu, R., Liu, Y.S., Zong, K.Q., Zou, D.Y., Deng, L.X., Tong, X.R., Hu, Z.C., Gao, S., 2013b. Micro-Geochemistry of Peridotite Xenoliths from Kuandian: Implications for Evolution of Lithospheric Mantle.
- Xu, W.L., Wang, F., Pei, F.P., Meng, E., Tang, J., Xu, M.J., Wang, W., 2013c. Mesozoic tectonic regimes and regional ore-forming background in NE China: Constraints from spatial and temporal variations of Mesozoic volcanic rock associations. *Acta Petrol. Sin.* 29 (2), 339–353.

- Xu, Y.G., Li, H.Y., Hong, L.B., Ma, L., Ma, Q., Sun, M.D., 2018. Generation of Cenozoic intraplate basalts in the big mantle wedge under eastern Asia. *Sci. China Earth Sci.* 61, 869–886.
- Yang, J.H., Sun, J.F., Zhang, M., Wu, F.Y., Wilde, S.A., 2012. Petrogenesis of silica-saturated and silica-undersaturated syenites in the northern North China Craton related to post-collisional and intraplate extension. *Chem. Geol.* 328, 149–167.
- Yin, A., 1996. A Phanerozoic palinspastic reconstruction of China and its neighboring regions. In: *Tectonic Evolution of Asia*.
- Yuan, X., Kind, R., Li, X., Wang, R., 2006. The S receiver functions: synthetics and data example. *Geophys. J. Int.* 165 (2), 555–564.
- Zhang, X.Z., Yang, B.J., Wu, F.Y., Liu, G.X., 2006. The lithospheric structure in the Hingmang-Jihe (Hinggan-Mongolia-Jilin-Heilongjiang) region, northeastern China. *Geol. China* 33 (4), 816–823.
- Zhang, R., Wu, Q., Sun, L., He, J., Gao, Z., 2014. Crustal and lithospheric structure of Northeast China from S-wave receiver functions. *Earth Planet. Sci. Lett.* 401, 196–205.
- Zhang, X.Z., Guo, Y., Zeng, Z., Fu, Q.L., Pu, J.B., 2015. Dynamic evolution of the Mesozoic-Cenozoic basins in the northeastern China. *Earth Sci. Front.* 22 (3), 88–98.
- Zhang, Y., Chen, L., Ai, Y., Jiang, M., 2019. Lithospheric structure beneath the central and western North China Craton and adjacent regions from S-receiver function imaging. *Geophys. J. Int.* 219 (1), 619–632.
- Zhao, L., 2005. Using shear wave splitting measurements to investigate the upper mantle anisotropy beneath the North China craton: distinct variation from east to west. *Geophys. Res. Lett.* 32 (10), L10309.
- Zhao, L., Zheng, T., 2007. Complex upper-mantle deformation beneath the North China craton: implications for lithospheric thinning. *Geophys. J. Int.* 3, 3.
- Zhao, D., Lei, J., Tang, R., 2004. Origin of the Changbai intraplate volcanism in Northeast China: evidence from seismic tomography. *Chin. Sci. Bull.* 49 (13), 1401–1408.
- Zhao, D., Maruyama, S., Omori, S., 2007. Mantle dynamics of Western Pacific and East Asia: insight from seismic tomography and mineral physics. *Gondwana Res.* 11, 120–131.
- Zheng, Y.F., Wu, F.Y., 2009. Growth and reworking of cratonic lithosphere. *Chin. Sci. Bull.* 54, 3347–3353.
- Zheng, J., O'reilly, S.Y., Griffin, W.L., Lu, F., Zhang, M., 1998. Nature and evolution of Cenozoic lithospheric mantle beneath Shandong peninsula, Sino-Korean craton, eastern China. *Int. Geol. Rev.* 40 (6), 471–499.
- Zheng, T., Chen, L., Zhao, L., Xu, W., Zhu, R., 2006. Crust–mantle structure difference across the gravity gradient zone in North China Craton: seismic image of the thinned continental crust. *Phys. Earth Planet. Inter.* 159 (1–2), 43–58.
- Zheng, T.Y., Zhao, L., Xu, W.W., Zhu, R.X., 2008. Insight into modification of North China Craton from seismological study in the Shandong Province. *Geophys. Res. Lett.* 35 (22).
- Zheng, X.F., Yao, Z.X., Liang, J.H., Zheng, J., 2010. The role played and opportunities provided by IGP DMC of China National Seismic Network in Wenchuan earthquake disaster relief and researches. *Bull. Seismol. Soc. Am.* 100 (5b), 2866–2872. <https://doi.org/10.1785/0120090257>.
- Zheng, T.Y., He, Y.M., Yang, J.H., Zhao, L., 2015. Seismological constraints on the crustal structures generated by continental rejuvenation in northeastern China. *Sci. Rep.* 5, 14995.
- Zhu, L.P., 2000. Crustal structure across the San Andreas fault, southern California from teleseismic converted waves. *Earth Planet. Sci. Lett.* 179 (1), 183–190.
- Zhu, R., Xu, Y., 2019. The subduction of the west Pacific plate and the destruction of the North China Craton. *Sci. China Earth Sci.* 62, 1340–1350.
- Zhu, R.X., Zheng, T.Y., 2009. Destruction geodynamics of the North China craton and its paleoproterozoic plate tectonics. *Sci. Bull.* 54 (19), 3354–3366.
- Zhu, R.X., Xu, Y.G., Zhu, G., Zhang, H.F., Xia, Q.K., Zheng, T.Y., 2012. Destruction of the North China Craton. *Sci. China Earth Sci.* 55, 1565–1587.